Research Journal of Engineering Technology and Medical Sciences (ISSN: 2582-6212), Volume 04, Issue 04, December-2021
Available at www.rjetm.in/

Increase the Efficiency of Photovoltaic Modules by Decreasing the Operating Temperature

Syed Saif Jibran[1], Dr Sohail Bux[2]
[1]MTech Scholar, [2]Professor
[1]Department of Mechanical Engineering, Agnos College of Technology, Bhopal, India
[2]Department of Mechanical Engineering, Agnos College of Technology, Bhopal, India
syedsaifjibran@gmail.com[1] buxsohail@gmail.com[2]

Abstract: Increase the efficiency and lifetime of photovoltaic modules by Decreasing the operating temperature. This can be accomplished by lessening the creation of waste hotness or by working on the dismissal of waste hotness. We tried, utilizing a mix of simu-lation and test, a few warm changes in each cate-violent. To anticipate working temperature and energy yield changes because of changes to the module, we carried out a material science based transient reproduction system put together essentially with respect to estimated properties. The best warm changes diminished the creation of waste hotness by mirroring unusable light from the phone or the module. Predictable with past outcomes and confirmed in this work through drawn out recreations, the ideal reflector brought about a yearly irradiance-weighted temperature decrease of 3.8 K for glasslike silicon (c-Si). Our outcomes delineate that more reasonable reflector ideas should offset impeding optical impacts with the expected warm impacts to understand the ideal energy creation advantage. Strategies working on warm conductivity or rear emissivity showed just humble upgrades of under 1 K. We likewise concentrated on a GaAs module, which utilizes high-productivity and high-subbandgap reflectivity to work at a yearly irradiance-weighted temperature 12 K cooler than that of a c-Si module under similar conditions.

Keywords: Photovoltaic Cells, Photovoltaic Frameworks, Beam Following, Solar Energy, Solar Chargers, Thermal Conductivity.

I. Introduction

All common types of solar cells lose efficiency with increasing temperature. Reducing a solar cell's temperature is one of the most effective ways of increasing its energy output. When they are deployed outdoors, solar cells are interconnected and packaged in a module [1]. Because many of the module's degradation mechanisms are thermally activated, reduced op- erating temperature is also an effective way of increasing the lifetime of a photovoltaic (PV) module [2]. A wide range of tech- niques have been investigated for cooling PV modules [3]–[7]. PV modules operate above the ambient temperature because they convert some of the incident sunlight into waste heat, for instance, due to absorption of subbandgap light or thermal- ization of carriers to the band edge. This production of waste heat is balanced by the rejection of heat, mainly by convec- tion and radiation. This suggests two classes of strategies for reducing operating temperature: 1) reduction of waste heat pro- duction and 2) improvement of waste heat rejection. In this work, we use a combination of computational modeling and outdoor experimentation to quantify the effect of several ther- mal modifications in each category. We do not consider dynamic temperature-reduction strategies, such as phase-change materi- als, desiccants, or active cooling by artificial forced convection.We also do not consider modifications to the forced and free convection occurring naturally outdoors.

II. Related Work

Different examinations showed that the presentation of a PV module relies not just upon its own properties like material, coating cover conveyance, and plate absorptance yet additionally on the genuine climate conditions like encompassing temperature, wind speed, and the unearthly conveyance of occurrence irradiance [2–5]. In any event, working under conditions like Standard Test Conditions (STC) sunlight based irradiance, the open air working effectiveness of multi-lucent PV was viewed as on normal 18.1% lower than the given STC productivity [6]. Ordinarily, every 1 ◦C of expanding temperature brings about a 0.5% decrease in effectiveness of glasslike PV module, while this figure of nebulous silicon PV module is 0.27% on normal [7]. One of the main isfortune factors, which adversely affect the last energy delivered by a PV framework, is the working temperature of the modules. This misfortune is addressed by the temperature misfortune coefficient, which relies upon the innovation of the module just as on the materials. In any case that those coefficient esteems are provided by producers, the cell working temperature should be known as an essential for assessing the all out warm misfortune. Consequently, precisely anticipating the open air working temperature assumes a significant part in displaying the energy yield of a PV framework. Thus, different investigations have been led to track down the most reasonable system for displaying the outside working calm of a PV module. As indicated by Skoplaki
furthermore, Palyvos, these models can be circulated in two principle classes: understood and express models [8].
The idea of verifiable models depends on the information on the warm properties of the PV module and their hotness move systems, which is the supposed consistent state energy balance. These models have demonstrated that they can decide the working temperature of a PV module under outside conditions. Be that as it may, this sort of model appears to confounded to execute by and by as they require the PV module to be in steadystate, which once in a while occurs under truly working conditions [9]. Additionally, since these models are made out of many variables that significantly rely upon module materials and neighborhood meteorology, different boundaries should be given at high accuracy to get the anticipated execution. This bother makes it hard to

move the implied models to other PV advances since they have basically been applied to glasslike silicon sun oriented cells. Quite possibly the most notable model depends on a basic energy balance proposed The unequivocal models, then again, stress the connection between cell temperature what's more, surrounding temperature just as the occurrence sun based radiation motion. Some of them consider the breeze speed, for example, while the others don't [11,14,15] in any case, in the two cases, the sun powered irradiance is the fundamental componentfor expanding the PV module temperature. Also, the temperature of the module is emphatically impacted by the warm protection of the module posterior coming about because of the rooftop mounting or building coordination [3,16]. Out of all models, the one set forward by Ruler utilizes a remarkable condition to depict the rising temperature brought about by episode irradiance and the decline in temperature brought about by the on location wind factor. Different scientists allude to utilizing ostensible working cell temperature (NOCT), which covers among implied and express techniques. The benefit of utilizing NOCT is that this boundary is normally provided by module producers, and the execution is straightforward. The inconvenience of this strategy is that the NOCT temperature is characterized under explicit meteorological conditions, which are hard to meet under genuine conditions. In addition, a few examinations showed that NOCT isn't consistent and differs by month, season, what's more, area [9,17]. That large number of models recorded above can foresee the temperature upsides of the module back surface of the PV cells for both moment esteems and hourly time steps. Notwithstanding, Segado et al. [9] observed that utilizing hourly info boundaries acquired a higher precision of the forecast contrasted with utilizing moment upsides of those boundaries. Also, past concentrates on showed that it is hard to track down a model, which can fulfill all PV module advances [9,18,19], while Koehl et al. [13] showed that the exactness of a warm model is likewise impacted by the on location conditions. Along these lines, one of the objects of this review is to work on the chance of computing PV module temperature by producing into account the results of its own warm latency, which unequivocally impacts the changing of the module temperature, particularly for areas where the sun powered irradiance and wind speed vacillate firmly. In this paper, two new module temperature models were proposed to anticipate the backsurface temperature of a PV module under open air working conditions. The appraisal considers boundaries related with the establishment site, like sun powered irradiance, encompassing temperature, wind speed, mounting setup, and span recording, alongside the PV cell material. The main model was accomplished by adjusting the technique depicted by Ruler, while the subsequent model depended on the possibility of the connection between module temperature and sun based illumination force on the PV surface. An examination between the proposed models and past models existing in the writing was executed to decide their unwavering quality.

III. Proposed Methodology

We concentrated on the impact of a few warm changes. For every one, we performed either virtual experiences, open air tests, or both. Two kinds of programmatic experience were utilized: a transient reenactment for up to an entire year in Golden, CO, USA, and a consistent state recreation at fixed irradiance. Both are portrayed in more detail in the accompanying. We utilized two measurements to look at the changes. Irradiance-weighted mean cell temperature transcend ambi-ent, ΔTw , gives a method of contrasting working temperature and accentuation on occasions when the creation of energy is high

$$\Delta T_w = \frac{\sum_t (T_{\text{module}} - T_{\text{ambient}})\, G_{\text{POA}}}{\sum_t G_{\text{POA}}}$$

ompare the ΔTw value between the reference module (see Section IIA) and the test module. The second metric we use to compare changes is cumulative DC power output, EDC, which we also evaluate against the base module. In the case of the GaAs module, due to the different sizes and technologies of the reference and test modules, the power generated by each module has been normalized based on its performance in standard test conditions (STC). For the modifications simulated with the transient model, we decomposed the total energy gain into “thermal” and “other” components. The total energy gain is calculated as the ratio of the additional energy generated by the modified module to the total energy generated by the reference module over the entire simulation period.

$$\sum_t P_{\text{baseline}} \gamma (T_{\text{modified}} - T_{\text{baseline}})$$

compare the ΔTw value between the reference module (see Section IIA) and the test module. The second metric we use to compare changes is cumulative DC power output, EDC, which we also evaluate against the base module. In the case of the GaAs module, due to the different sizes and technologies of the reference and test modules, the power generated by each module has been normalized based on its performance in standard test conditions (STC). For the modifications simulated with the transient model, we decomposed the total energy gain into “thermal” and “other” components. The total energy gain is calculated as the ratio of the additional energy generated by the modified module to the total energy generated by the reference module over the entire simulation period.

A. Baseline Modules

Every temperature decrease was measured corresponding to a pattern module. We utilized various kinds of gauge modules in reproductions to guarantee a reasonable correlation of every change and in tests relying upon information accessibility. In the

accompanying portrayals, effectiveness alludes to the module's deliberate STC productivity during our tests and additionally reproductions.

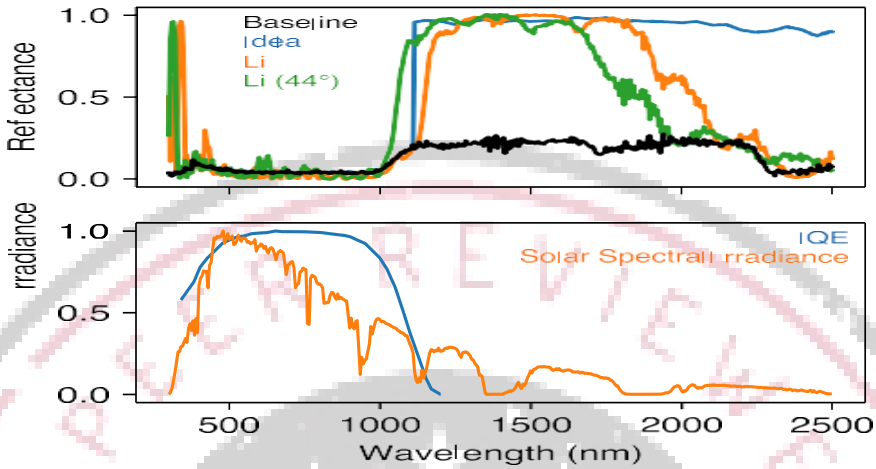

Fig. 1. Total reflectance (top) for various simulated modules is shown with the normalized solar spectrum and the IQE

Module A was a mimicked 17.1% productive translucent sili-con module with ordinary bundling materials: glass front, ethylene vinyl acetic acid derivation (EVA) epitome, and white polymer backsheet. To work on the calculation for some reproductions of a whole year of administration, module A had no edge and had a uniform layer addressing the cells.
Module B was a recreated glasslike silicon module dependent on module A, yet with an aluminum edge and individual cells. It addressed a 2-D get segment through a module with six sections of cells. Module B was utilized distinctly for consistent state sim-ulations. Module C was a genuine copper indium gallium diselenide (CIGS) module with glass on both the front and back surfaces. This module was made in 2014 and was the main module with an antireflective covering on the front surface of the glass. Module D was a genuine and reproduced 60-cell (1.6 m2), 15% proficient glasslike silicon module with traditional packag-ing materials and an aluminum outline. This module was made in 2012. Module E was a genuine and recreated 36-cell (0.6 m2), 17% productive glasslike silicon module with traditional undling materials and an aluminum outline. This module was made in 2016. Module F was a truly 36-cell (0.6 m2), 11% effective crys-talline silicon module with regular bundling materials and an aluminum outline. This module was made during the 1990s.

B. Thermal Modifications

We changed the standard modules to execute each ther-mal adjustment. The alterations are numbered by Table II.

1) Efficiency and Temperature Coefficient: While effectiveness and temperature coefficient are not ordinarily free boundaries, we recreated their impacts on working temperature to set up the affectability of temperature expectation on these boundaries. Utilizing module A, we recreated expanding module productivity by 5% (relative), from 17.1% to 18.0% (alteration 1). We independently recreated splitting the temperature coefficient, from 0.39 to 0.20% K−1 (adjustment 2).
2) Front Optical Modifications: Using module A, we sim-ulated the expansion of an ideal subbandgap reflector, reflecting 100% of the power in the sun based range beneath the cell bandgap and sending 100% of the power over the cell bandgap. This ideal reflector is situated between the front glass and front encapsulant (changes 3–5). The recreated reflectances of module An and of the module with the ideal subbandgap reflec-pinnacle are displayed in Fig. 1. Some infrared retention in the glass is as yet clear for this adjustment on the grounds that the best reflector is at the glass/EVA interface; accordingly, all occurrence light collaborates with the glass. We likewise mimicked the expansion of a normal antireflective covering on the glass by including 99 nm of the covering portrayed in [8, Sec. 3.2] adjustments 4 and 6). To comprehend the most outrageous conceivable exhibition of antireflec-tion draws near, we displayed an optimal antireflective covering on the front glass, which accomplishes solidarity transmission at the air/glass interface (alterations 5 and 7).
3) Back Surface Reflectance: Using module C, we per-framed open air testing of the utilization of a high-reflectivity covering to the module's back surface (change 14). The covering expanded the hemispherical reflectance of the back sur-face from 44% to 89% of the power in the sun oriented range and expanded the emissivity of the back surface from 0.88 to 0.93.
4) Packaging Emissivity: Using module A, we mimicked in-wrinkling the emissivity of the front surface to 1.0 (adjustment 15), the back surface to 1.0 (change 16), and both front and back surfaces to 1.0 (alteration 17). Since some backsheet items contain a foil layer that diminishes their emissivity, we likewise reenacted the decrease of the back surface emissivity to 0.75 (adjustment 18).

5) Packaging Thermal Conductivity: Using module A, we reproduced multiplying the through-plane warm conductivity (k) of the backsheet (adjustment 19). We likewise reenacted multiplying the through-plane conductivity of both the back encapsulant and the backsheet (alteration 20). Utilizing module D, we performed outside testing of the impact of almost multiplying the through-plane k of the back encapsulant and backsheet materials from 0.21 to 0.41 W m−1 K−1 (mod-ification 21). This was finished by correlation with a module that was generally indistinguishable from module D, yet was initially fab-ricated with uncommon back bundling materials. These materials didn't contain any layers, like metal or graphite, that would be relied upon to present solid anisotropy in heat conduction.

Utilizing module B, we recreated the presentation of a 100-μm layer of aluminum in the backsheet (adjustment 22) by increas-ing k of the backsheet to 0.31 W m−1 K−1 the through-plane way and 40 W m−1 K−1 the in-plane way and re-ducing the backsheet emissivity to 0.75.

Utilizing module E, we reenacted and tried outside the promotion dition of two layers of warm protection to the back surface of the module (changes 12 and 23). The back surface of the external layer of protection was painted with dark paint (so-lar assimilation 0.95). This treatment was made to one module with the subbandgap reflector film and one without. While not a temperature-decrease procedure itself, the protection served to show the subbandgap reflector film under thermally promotion section conditions. These conditions imitated those experienced in a rooftop incorporated application, where no convection or radia-tion heat move acts straightforwardly on the back surface of the mod-ule. Recreating the warm protection additionally served to approve the model's viability for making temperature and energy forecasts dependent on estimated properties.

C. Transient Photovoltaic System Thermal Model

We reenacted the working temperature of sun powered cells in a PV framework for up to a whole year in Golden, CO, USA, utilizing the limited component strategy [13]. This model was utilized for sim-ulations of modules A, D, and E. The reproduction structure is outlined in Fig. 2. This reproduction structure varies from other exact or phenomenological models, where the objec-tive is foreseeing temperature for a specific PV framework dependent on surrounding conditions. All things being equal, this current model's goal is to pre-dict changes in PV module temperature because of changes to the PV module itself. All things considered, it is physical science based and utilizes only estimated material properties.

1) Geometry: We utilized a 2-D model of the cross segment (the plane containing the "up" and "north" vectors) of a fixed-slant PV framework. The math of the model is shown schematically in Fig. 3. Three lines of modules were reenacted, with conduction expressly recreated in the center module line and the surface temperatures of the front and back line compelled to coordinate with the surface temperatures of the center module. This addressed a framework with vastly many lines. Modules were demonstrated as a plane divider; the edge, interconnects, and holes between cells.

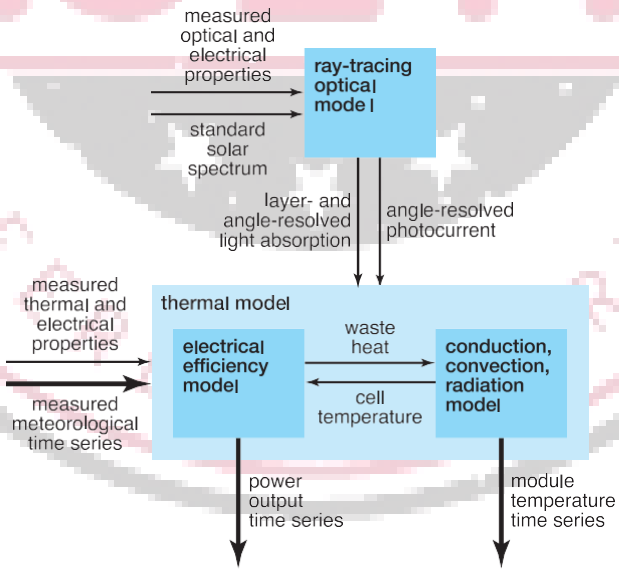

Fig. 2. Diagram illustrating our simulation approach is shown.

were dismissed in the model math. Mathematical boundaries are summed up in Table I. Despite the fact that we thought about various sizes of modules, this size contrast minorly affected reproduction results. Scaling the module tallness and line pitch somewhere around half or up by 25% came about in a < 0.01 K change to ΔTw . In this manner, we utilized a similar reproduction math for each situation.

2) Optics: The hotness to be conveyed to each layer of the mod-ule was determined in a frightfully settled manner utilizing beam following that likewise represents reasonable impacts in flimsy movies [14], [15]. This methodology empowered the reproduction of impacts on vari-ous length scales, from flimsy film obstruction to cell finishing. The occurrence range was thought to be corresponding to the AM1.5G range, and the hotness ingested in each layer was relative to episode irradiance estimated utilizing a thermopile pyranometer shifted at 40◦. The optical recreation was completed at 11◦ strides in point of rate from 0◦ to 88◦. For every occurrence point, we determined the absolute energy consumed in every module layer. We likewise determined the hemispherical normal for each layer's all out energy ingested; this was utilized to reproduce the impacts of the diffuse part of sun based radiation. For each point and the isotropic case, we likewise determined the fragmentary change in photocurrent comparative with the ordinary rate pattern case from the joining of the frightfully settled retention in the Si layer (cell), got from the beam following reenactments, increased by a commonplace c-Si inside quantum effectiveness (IQE) [11]. IQE alludes to the electrical assortment effectiveness with which photocarriers made by photons of a given frequency are col-lected. The IQE does exclude optical misfortunes. We use it here rather than the outer quantum effectiveness to try not to twofold include optical misfortunes represented in the beam following simu-lations. The subsequent photocurrent factor was utilized to changethe module efficiency for the subsequent transient thermal sim-ulations.The light incident on the module's back surface was as- sumed to be proportional to the plane-of-array irradiance. In simulations, this energy was delivered to the module back sur- face according to the surface's absorptivity. The back-side irra-diance fraction, derived from experimental data on our testbed,and module back surface absorptivity are shown in Table I.

3) Conduction: Heat was delivered uniformly to each layer of the thermal model according to results from the ray-tracing model. In the cell layer, the PV cell's temperature-dependent efficiency was evaluated at the cell layer's average tempera- ture using the power temperature coefficient model [16]. This efficiency was modified by the angle-dependent factor calcu- lated using the optical model and was used to sink the amount of energy that was converted to electricity. Material properties relevant to the conduction simulation are shown in Table I.

4) Convection: We simulated convection on the front and rear module surfaces using Newton's law of cooling. We used the convection correlation for a flat plate in parallel flow at the wind speed measured by an ultrasonic anemometer and with measured ambient temperature [17]. Because this correlation underestimates convection for PV systems, we modified it by scaling the characteristic length to match experimental data at our facility. This scale factor is the only fitting parameter in the model, and the same value (0.56) was used in every simulation in this work.

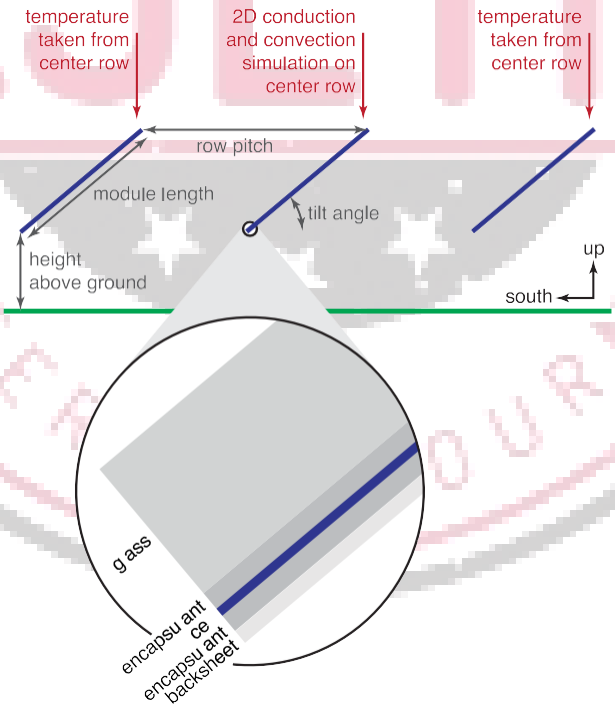

Fig. 3. Geometry used in the transient PV system thermal model

5) Radiation: We assumed the module surfaces and ground surface to be gray bodies with constant emissivity values. The ground surface was modeled as concrete. The sky was modeled as distant black surroundings with uniform tempera- ture. Effective ground and sky temperatures were derived from long-wavelength radiation measurements from downward- and upward-facing

pyrgeometers at a nearby meteorological station [18]. Areas of ground covered by the PV system's shadow were assumed to be at the ambient temperature. The view factors be- tween surfaces in the model were calculated using the hemicube method [13].

D. Steady-State Photovoltaic Module Model With a Frame

To simulate module B and the modified version of module B (modification 22), we used a 2-D finite-element model of a PV module including a cross section of the aluminum frame bonded to the laminate with silicone adhesive. The frame and adhesive were omitted from the transient simulation for sim- plicity, but were required to investigate the potential for the frame to act as a cooling enhancement. We simulated steady- state conditions at 1000 W m−2 with radiation and convection conditions typical for this irradiance in our location. We ap- plied an 8.2 W m−2 K−1 convection coefficient with 16.9 °C surroundings on module and outer frame surfaces and radiation with uniform 14.9 °C surroundings on module front and back surfaces only. The steady-state simulation was representative of operation in high-irradiance conditions, when the potential for temperature reduction is highest and when the benefit of a tem- perature reduction is greatest. As such, the results were not used to predict an energy benefit, but instead to screen for whether a frame modification could be promising.

TABLE I
MATERIAL PROPERTIES AND OTHER PARAMETERS FOR THE THERMAL MODEL

parameter	material	value	units	source
emissivity	low-iron solar glass	0.88		measured
emissivity	polymer backsheet	0.87		measured
emissivity	polymer/aluminum/polymer backsheet	0.75		measured
emissivity	concrete	0.88		[17]
thermal conductivity	low-iron solar glass	1	$W\ m^{-1}\ K^{-1}$	[19]
thermal conductivity	EVA	0.26	$W\ m^{-1}\ K^{-1}$	measured
thermal conductivity	silicon solar cell	148	$W\ m^{-1}\ K^{-1}$	[20]
thermal conductivity	polymer backsheet	0.26	$W\ m^{-1}\ K^{-1}$	measured
thermal conductivity	silicone adhesive	0.2	$W\ m^{-1}\ K^{-1}$	[21]
thermal conductivity	polystyrene insulation (inner)	0.029	$W\ m^{-1}\ K^{-1}$	[22]
thermal conductivity	polyisocyanurate insulation (outer)	0.022	$W\ m^{-1}\ K^{-1}$	[23]
density	low-iron solar glass	2500	$kg\ m^{-3}$	[19]
density	EVA	960	$kg\ m^{-3}$	[24]
density	silicon solar cell	2330	$kg\ m^{-3}$	[25]
density	polymer backsheet	1200	$kg\ m^{-3}$	[25]
density	polystyrene insulation (inner)	20.8	$kg\ m^{-3}$	[22]
density	polyisocyanurate insulation (outer)	32	$kg\ m^{-3}$	[23]
specific heat	low-iron solar glass	720	$J\ kg^{-1}\ K^{-1}$	[19]
specific heat	EVA	2090	$J\ kg^{-1}\ K^{-1}$	[24]
specific heat	silicon solar cell	677	$J\ kg^{-1}\ K^{-1}$	[25]
specific heat	polymer backsheet	1250	$J\ kg^{-1}\ K^{-1}$	[25]
specific heat	polystyrene insulation (inner)	1200	$J\ kg^{-1}\ K^{-1}$	[26]
specific heat	polyisocyanurate insulation (outer)	1453	$J\ kg^{-1}\ K^{-1}$	[26]
thickness	low-iron solar glass	3.2	mm	[19]
thickness	EVA	0.4	mm	measured
thickness	silicon solar cell	0.15	mm	measured
thickness	polymer backsheet	0.3	mm	measured
thickness	polystyrene insulation (inner)	25	mm	measured
thickness	polyisocyanurate insulation (outer)	51	mm	measured
module length		1	m	
height above ground		0.5	m	
row pitch		1.53	m	
tilt		40	degrees	
azimuth		180	degrees	
back irradiance fraction		0.1		measured
back solar absorptivity		0.33		measured
plane-of-array irradiance		time series		measured
ambient temperature		time series		measured
wind speed		time series		measured
effective sky temperature		time series		measured
effective ground temperature		time series		measured

E.Outdoor Testing

For outdoor testing, modules were deployed in Golden, CO, USA, tilted at 40◦ and oriented south. I–V curves and module rear surface temperature measurements were collected auto- matically every 5 min on modules C, D, and E and every 15 min on module F and the GaAs module. Surface temperature measurements were made with thin type-T thermocouples ad- hered to module surfaces using a polyester tape.The outdoor testbed was equipped with thermopile pyranome- ters. To eliminate temperature inaccuracy introduced by adding the reflective coating to module C between the temperature probe and the module's back surface, we derived cell tempera- ture from irradiance and Voc for module C. The GaAs module and module F were deployed together for one year, and we used their back surface temperatures assuming like packaging materials in each module. frame to act as a cooling enhancement. We simulated steady- state conditions at 1000 W m^{-2} with radiation and convection conditions typical for this irradiance in our location. We ap- plied an 8.2 W m^{-2} K^{-1} convection coefficient with 16.9 °C surroundings on module and outer frame surfaces and radiation with uniform 14.9 °C surroundings on module front and back surfaces only. The steady-state simulation was representative of operation in high-irradiance conditions, when the potential for temperature reduction is highest and when the benefit of a tem-perature reduction is greatest. As such, the results were not used to predict an energy benefit, but instead to screen for whether aframe modification could be promising.

TABLE II

			baseline module	ΔT_w (K) improvement	relative energy improvement		
					total	thermal contribution	other contribution
1	efficiency increase	increase efficiency 5% (relative)	A	0.2[s]	0.054[s]	0.001[s]	0.053[s]
2	temperature coefficient decrease	decrease temperature coefficient by half	A	0.1[s]	0.023[s]	<0.001[s]	0.023[s]
3	front optical modification	ideal sub-bandgap reflector behind glass	A	3.8[s]	0.017[s]	0.016[s]	0.001[s]
4	front optical modification	ideal sub-bandgap reflector with ordi- nary antireflective coating	A	3.4[s]	0.038[s]	0.014[s]	0.024[s]
5	front optical modification	ideal sub-bandgap reflector with ideal antireflective coating	A	2.8[s]	0.086[s]	0.011[s]	0.074[s]
6	front optical modification	ordinary antireflective coating	A	−0.4[s]	0.022[s]	−0.002[s]	0.023[s]
7	front optical modification	ideal antireflective coating	A	−1.2[s]	0.068[s]	−0.005[s]	0.072[s]
8	front optical modification	reflector on outside surface (Li)	A	3.4[s]	0.019[s]	0.014[s]	0.005[s]
9	front optical modification	reflector on outside surface (Li omni- directional)	A	2.3[s]	0.015[s]	0.009[s]	0.006[s]
10	front optical modification	infrared reflector film on front surface	C	3[e,p]	−0.10[e,p]		
11	front optical modification	infrared reflector film on front surface	E	4[e,p]	−0.08[e,p]		
12	front optical modification	infrared reflector film on front surface with insulated back	E	−8[e,p]	−0.11[e,p]		
13	front optical modification	GaAs module	F	12[e]	0.09[e]		
14	increase back reflectance	reflective coating on back surface	C	1.7[e,p]	0.01[e,p]		
15	emissivity change	front emissivity 1.0	A	0.8[s]	0.004[s]	0.004[s]	0[s]
16	emissivity change	back emissivity 1.0	A	0.5[s]	0.002[s]	0.002[s]	0[s]
17	emissivity change	front and back emissivity 1.0	A	1.3[s]	0.006[s]	0.006[s]	0[s]
18	emissivity change	back emissivity 0.75	A	−0.5[s]	−0.002[s]	−0.002[s]	0[s]
19	thermal conductivity change	double through-plane k in backsheet	A	0.1[s]	<0.001[s]	<0.001[s]	0[s]
20	thermal conductivity change	double through-plane k in backsheet and back encapsulant	A	0.1[s]	0.001[s]	0.001[s]	0[s]
21	thermal conductivity change	isotropic 1.95× increase in backsheet and encapsulant k	D	0.1[s] <1[e]	<0.01[s] <0.01[e]		
22	thermal conductivity change	addition of 100-μm aluminum film in backsheet	B	0.2[s,t]	<0.01[s,t]		
23	thermal conductivity change	insulated back	E	−13[s,p] −12[e,p]	−0.05[s,p] −0.06[e,p]		

RESULTS OF THERMAL MODIFICATIONS

III. RESULTS AND DISCUSSION

Test yield of the warm model is contrasted and out-entryway estimations for module E and the thermally protected variant of module E (adjustment 23) in Fig. 4. The recreation shows great concurrence with the examination over a scope of con-ditions; notwithstanding, the reenacted temperature is marginally one-sided over the investigation under high-temperature conditions and be-low the analysis under low-temperature conditions. The ther-mal model has just a solitary fitting boundary, the trademark length scaling factor for convection heat transfer, and this pa- rameter was fitted using experimental data from a different PV system during a different time period. There is disagreement about the appropriate functional form for convection heat trans-fer in PV [27]. The available relationships use parameters that may require refitting according to system-specific

features or geographic location [28]. To keep the model a mainly physics- based prediction tool rather than a fitted model, we chose a very simple convection relationship, which does not include free convection. Our results are, thus, a compromise between modelaccuracy and the number of fitting parameters. There may be cases, such as locations where free convection dominates over forced convection, where a more complex convection function would be required. The sample data and the comparisons be- tween simulation (superscript "s") and experiment (superscript"e") shown in rows 21 and 23 of Table II demonstrate that the thermal model can make good predictions based only on mea- sured properties. Results from the thermal modifications are summarized in Table II and discussed in detail in the following. Results are given as differences in ΔT_w or fractional difference in E_{DC} be- tween the indicated baseline module and the module with the change described in the "variation" column. A positive value indicates an improvement, either a temperature reduction or anenergy increase. Values for simulation (superscript "s") and ex-periment (superscript "e") are given where available. Results from partial-year simulations and experiments (superscript "p") may not represent full-year performance due to seasonal ef- fects. The steady-state simulation is marked with superscript "t." Where a "<" symbol is present, it shows that the result was between zero and the indicated value. The "thermal" and "other" components of energy benefit are illustrated for a subset of the modifications in Fig. 5.

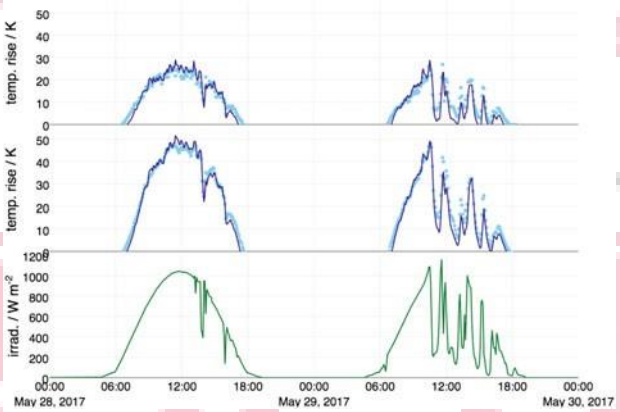

Fig. 4. Temperature rise above ambient for module E (top plot) and the insulated-back version of module E (middle plot).

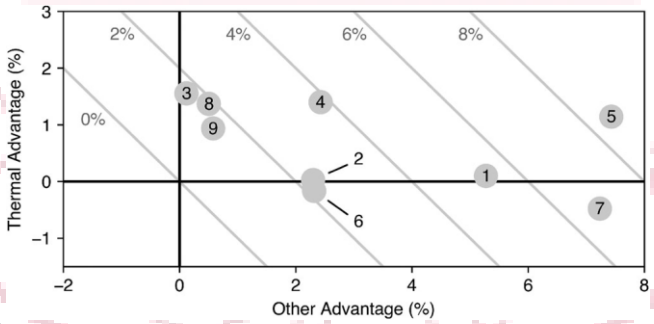

Fig. 5. Energy advantage of several of the module modifications is decom- posed into "thermal" and "other" components.

A. Efficiency and Temperature Coefficient

We considered the effects of efficiency and temperature co- efficient improvement for easy comparison to the other thermal modifications. The results are shown in Table II and Fig. 5. Improving efficiency from 17.1% to 18% (modification 1) or halving of the temperature coefficient (modification 2) each only reduced the production of waste heat in the cell by about 1%, giving a small effect on operating temperature. While these changes result in major improvements to energy production, they do not cause major temperature reductions.

B. Front Optical Modifications

The results from the addition of an ideal subbandgap reflector (modification 3) are shown in Table II and Fig. 5. The ideal reflector gave a substantial temperature reduction. Considering only high-irradiance conditions, this reduction approached 5 K, consistent with previous results [29] Table II and Fig. 5 also show results from combinations of antireflective coatings

and subbandgap reflective coatings (mod- ifications 4–7) illustrating the competing effects of increasing energy conversion using antireflection and decreasing tempera- ture using subbandgap reflection. Adding an antireflective coat- ing alone reduces the module's subbandgap reflectivity and raises its temperature (modifications 6 and 7). Our results show that adding a subbandgap reflector (modifications 4 and 5) can counteract this effect and further improve energy gain.A comparison of the results of the ideal subbandgap reflector (modification 3) and the ideal antireflection coating (modifica- tion 7) indicates that there is substantially more photocurrent gain than thermal improvement to be realized through front op- tical modifications. However, the 1.6% improvement in energy yield available (for this particular simulated PV system and lo- cation) with the subbandgap reflector is appreciable. It is also important to note that infrared performance of antireflection ap- proaches should be considered. As shown in Table II and Fig. 5, introducing the ideal antireflection coating has detrimental ther- mal effect, which should be considered and managed in the design of such coatings.

Results from simulations of the multilayer stack proposed by Li (modifications 8 and 9) shown in Table II and Fig. 5 indicate that both coatings realize an operating temperature re- duction. The omnidirectional version of the coating (modifica- tion 9) trades a reduced thermal benefit for a small benefit in above-bandgap performance. It is important to note that this is not a universal result; it depends on the location (i.e., weather and irradiance) and configuration of the PV system. However, it highlights an important challenge with thin-film stack reflectors that reflection bands shift to shorter wavelengths at off-normal incidence. Thus, a balance must be struck between the position of the short-wavelength edge of the normal-incidence reflec- tion band and the off-angle transmission above the solar cell's bandgap. The difference in performance between modification 8 and 9 in this particular fixed-tilt application illustrates this tradeoff.Outdoor tests of the polymer reflector film (modifications 10 and 11) showed a substantial temperature benefit. However, be- cause the filter reflected a portion of the solar spectrum's power above the cell's bandgap, the treatment resulted in a current reduction that caused a loss in energy. We anticipate that this film would have better performance inside the module due to the elimination of the reflective interface between the film and air. We attribute the small discrepancy in performance between modifications 10 and 11 to the different weather (including spec- trum, irradiance, angle of incidence, and temperature) during the two partial-year tests and the different spectral and angular re- sponses of the modules. Comparing the insulated-back module (modification 23) with the insulated-back module with infrared reflector film (modification 12) shows a greater thermal benefit than application of the film to an open-back module (about a 5 K temperature decrease). This illustrates that the strategy of reducing the amount of waste heat produced in the module gives a thermal benefit that becomes larger when the removal of heat from the module is compromised.

C. Back Surface Reflectance

Adding a reflective coating to reject light incident on module C's back surface (modification 14) yielded a substantial temper- ature decrease. This treatment is promising because it may be simpler to engineer a weatherproof broadband reflective coating than a selective reflector with high transmission of light usable to the cell. This modification applies to modules, like CIGS and CdTe, that normally have a low-reflectivity back surface.

D. Packaging Emissivity

Unlike the emissivity of bare silicon or metal, the emissivity of PV module packaging materials is relatively high. Further increasing the emissivity of only one surface (modifications 15 and 16) had a modest effect, consistent with previous results [29], [30]. Increasing both outside surface emissivity values (modification 17) gave a larger effect, but provided less than a 1% increase in energy output. Reducing emissivity by using a backsheet containing an aluminum layer (modification 18) resulted in a small temperature increase due to poorer radia- tion heat transfer. In an opaque backsheet material, increasing emissivity without increasing absorption of sunlight is possible. However, it may be difficult to produce a low-cost weatherproof coating for glass that increases the module's front emissivity.

E. Packaging Thermal Conductivity

Because it is relatively thin and the energy flux density across it is relatively small, the through-plane thermal resistance of PV packaging materials is relatively low. Reducing this thermal resistance further (modifications 19 and 20) had a very small effect in simulations. Increasing the k of back packaging can cause the module back surface temperature to increase even if the cell temperature has decreased. In outdoor testing of the module with high-thermal- conductivity back packaging (modification 21), we detected a difference in surface temperature small enough that we could not conclude that there was a substantial reduction in cell tem- perature. A simulation of the same test matched this result.An aluminum frame acts as a surface area enhancement and, combined with a backsheet having high in-plane k (modifica- tion 22), increases removal of heat at the module edges. Our simulation predicted the maximum benefit, occurring in sunny conditions and with unobstructed convection on the outer sur- faces of the module frame. Adding a foil layer cooled the cell adjacent to the frame by 0.7 K but reduced radiative heat transfer due to the metal-containing backsheet led to a net temperature increase.Adding insulation to the module back surface (modification 23) caused a major increase in operating temperature and re- duction in energy production. The simulation was a satisfactory match to the experiment and shows the disadvantage of mount- ing configurations with limited heat transfer from the module back surface.

F. Extension of Module Service Life

While it is impossible to explicitly predict the service life of a PV module, among the module's many parallel and serial degradation mechanisms are several that are thermally activated. A rough approximation of overall degradation is possible by using the Arrhenius equation to model degradation as a single thermally activated process. We calculated time to failure

TF as where Ea is activation energy, kb is the Boltzmann constant, T is module temperature, Δt is the simulation time step, and the denominator is summed over all time steps of the thermal simulation. Because we make only relative comparisons of TF, the value of the preexponential factor A is arbitrary. There is not a well-established activation energy for the overall degrada- tion process, but we can make a crude assessment of the lifetime extension offered by temperature reduction by assuming a range of effective activation energy values from 0.6 to 2 eV [2]. Un- der these simple approximations, the ideal subbandgap reflector can yield an increase in TF ranging from 26% to 200%. This is a major simplification that neglects the effects of moisture, ultraviolet light, mechanical stress, other driving forces for fail- ure, and the interactions among concurrent failure mechanisms. However, we use the result to illustrate that temperature reduc- tion can have a role beyond improved energy production.

CONCLUSION

With PV module temperature can be reduced through reductions in waste heat generation or improvements in waste heat rejec- tion. We found that strategies reducing waste heat generation generally performed better than those improving waste heat re- jection. Changes to thermal conductivity and back emissivity yielded only modest temperature changes. Strategies reducing the irradiance-weighted temperature rise of PV modules by more than 1 K included rejecting subbandgap light from the module or cell, reflecting light from the module back surface, and giving both front and back surfaces ideal emissivity. Optical modifica- tions that alter the module's reflection of light must balance their thermal effects with nonthermal optical effects to maximize the production of energy.

References

[1] J. Nelson, *The Physics of Solar Cells*. London, U.K.: Imperial College Press, 2003.
[2] S. Kurtz *et al*., "Evaluation of high-temperature exposure of photovoltaic modules," *Prog. Photovolt., Res. Appl.*, vol. 19, no. 8, pp. 954–965, 2011.
[3] M. Hasanuzzaman, A. Malek, M. Islam, A. Pandey, and N. Rahim, "Global advancement of cooling technologies for PV systems: A review," *Sol. Energy*, vol. 137, pp. 25–45, 2016.
[4] S. Sargunanathan, A. Elango, and S. T. Mohideen, "Performance en- hancement of solar photovoltaic cells using effective cooling methods: A review," *Renewable Sustain. Energy Rev*., vol. 64, pp. 382–393, 2016.
[5] J. Siecker, K. Kusakana, and B. Numbi, "A review of solar photovoltaic systems cooling technologies," *Renewable Sustain. Energy Rev*., vol. 79,pp. 192–203, 2017.
[6] A. Shukla, K. Kant, A. Sharma, and P. H. Biwole, "Cooling methodologies of photovoltaic module for enhancing electrical efficiency: A review," *Sol. Energy Mater. Sol. Cells*, vol. 160, pp. 275–286, 2017.
[7] M. R. Vogt *et al.*, "Reduced module operating temperature and increasedyield of modules with PERC instead of Al-BSF solar cells," *IEEE J. Photovolt.*, vol. 7, no. 1, pp. 44–50, Jan. 2017.
[8] M. R. Vogt, "Development of physical models for the simulation of optical properties of solar cell modules," Ph.D. dissertation, Faculty Math. Phys., Gottfried Wilhelm Leibniz Univ. Hannover, Hannover, Germany, 2015.
[9] W. Li, Y. Shi, K. Chen, L. Zhu, and S. Fan, "A comprehensive photonic approach for solar cell cooling," *ACS Photon.*, vol. 4, no. 4, pp. 774–782,2017.
[10] J. Kischkat *et al.*, "Mid-infrared optical properties of thin films of alu- minum oxide, titanium dioxide, silicon dioxide, aluminum nitride, and silicon nitride," *Appl. Opt.*, vol. 51, no. 28, pp. 6789–6798, Oct. 2012.
[11] C. Tool *et al*., "17% mc-Si solar cell efficiency using full in-line process- ing with improved texturing and screen-printed contacts on high-ohmic emitters," in *Proc. 20th Eur. Photovolt. Sol. Energy Conf. Exhib*., 2005, vol. 6, p. 10.
[12] T. J. Silverman *et al*., "Outdoor performance of a thin-film gallium- arsenide photovoltaic module," in *Proc. 39th IEEE Photovolt. Spec. Conf.*, 2013, pp. 103–108.
[13] *COMSOL Heat Transfer Module User's Guide*, COMSOL, Los Angeles,CA, USA, 2017.
[14] I. Subedi, T. J. Silverman, M. Deceglie, and N. J. Podraza, "Impact of infrared optical properties on crystalline Si and thin film CdTe solar cells," in *Proc. 44th IEEE Photovolt. Spec. Conf.*, 2017.
[15] I. Subedi, T. J. Silverman, M. Deceglie, and N. J. Podraza, "Al+Si interface optical properties obtained in the Si solar cell configuration," *Phys. StatusSolidi A, Appl. Mater. Sci.*, vol. 214, no. 12, 2017, Art. no. 1700480.
[16] B. Marion, "Comparison of predictive models for photovoltaic mod-ule performance," in *Proc. 33rd IEEE Photovolt. Spec. Conf.*, 2008,pp. 1–6.
[17] F. P. Incropera and D. P. DeWitt, *Fundamentals of Heat and Mass Transfer*,5th ed. Hoboken, NJ, USA: Wiley, 2002.
[18] A. Andreas and T. Stoffel, "NREL solar radiation research laboratory (SRRL): Baseline measurement system (BMS)," Nat. Renewable EnergyLab., Golden, CO, USA, Tech. Rep. DA-5500-56488, 1981.
[19] *Solite Patterned Glass Datasheet*, AGC Solar, Kingsport, TN, USA, 2012.
[20] Z. Lu and Q. Yao, "Energy analysis of silicon solar cell modules based on an optical model for arbitrary layers," *Sol. Energy*, vol. 81, no. 5,pp. 636–647, 2007.
[21] *Silicon-Based Photovolt. Solutions*, Dow Corning, Auburn, MI, USA, 2015.
[22] *Foamular Extruded Polystyrene Insulation Datasheet*, Owens Corning, Toledo, OH, USA, 2011.
[23] *Thermasheath-3 Insulation for the Building Envelope*, Rmax Operating, Dallas, TX, USA, 2015.
[24] *Photocap Solar Cell Encapsulants Technical Manual*, Specialized Tech-nology Resources, Enfield, CT, USA, 2015.
[25] A. Jones and C. Underwood, "A thermal model for photovoltaic systems," *Sol. Energy*, vol. 70, no. 4, pp. 349–359, 2001.
[26] *Isolparma Thermal Insulation Boards Datasheet*, Isolparma Srl, Padova,Italy, 2007.
[27] E. Skoplaki and J. Palyvos, "Operating temperature of photovoltaic mod-ules: A survey of pertinent correlations," *Renewable Energy*, vol. 34, no. 1, pp. 23–29, 2009.
[28] E. Barykina and A. Hammer, "Modeling of photovoltaic module tempera-ture using Faiman model: Sensitivity analysis for different climates," *Sol. Energy*, vol. 146, pp. 401–416, 2017.

[29] X. Sun *et al.*, "An optics-based approach to thermal management of pho- tovoltaics: Selective-spectral and radiative cooling," *IEEE J. Photovolt.*,vol. 7, no. 2, pp. 566–574, Mar. 2017.
[30] A. Gentle and G. Smith, "Is enhanced radiative cooling of solar cell mod-ules worth pursuing?" *Sol. Energy Mater. Sol. Cells*, vol. 150, pp. 39–42,2016.